PRIFYSGOL BANGOR / BANGOR UNIVERSITY

Thermal conductivity variation in uranium dioxide with gadolinia additions

Qin, Meng; Middleburgh, Simon; Cooper, M. W. D.; Rushton, Michael; Puide, Mattias; Kuo, E. Y.; Grimes, Robin W.; Lumpkin, Gregory R.

Journal of Nuclear Materials

DOI:
https://doi.org/10.1016/j.jnucmat.2020.152258

Published: 01/11/2020

Peer reviewed version

Cyswllt i'r cyhoeddiad / Link to publication

Dyfyniad o'r fersiwn a gyhoeddwyd / Citation for published version (APA):
Qin, M., Middleburgh, S., Cooper, M. W. D., Rushton, M., Puide, M., Kuo, E. Y., Grimes, R. W., & Lumpkin, G. R. (2020). Thermal conductivity variation in uranium dioxide with gadolinia additions. *Journal of Nuclear Materials*, *540*, [152258]. https://doi.org/10.1016/j.jnucmat.2020.152258

Hawliau Cyffredinol / General rights
Copyright and moral rights for the publications made accessible in the public portal are retained by the authors and/or other copyright owners and it is a condition of accessing publications that users recognise and abide by the legal requirements associated with these rights.

• Users may download and print one copy of any publication from the public portal for the purpose of private study or research.
• You may not further distribute the material or use it for any profit-making activity or commercial gain
• You may freely distribute the URL identifying the publication in the public portal ?

Take down policy
If you believe that this document breaches copyright please contact us providing details, and we will remove access to the work immediately and investigate your claim.

05. May. 2023

Thermal conductivity variation with Gd accommodation in Gd-doped UO_2 using NEMD method

M.J. Qin[a,*], S.C. Middleburgh[b,c], M.W.D. Cooper[d], M.J.D. Rushton[c,e], M. Puide[b], E.Y. Kuo[a], R.W. Grimes[e], G.R. Lumpkin[a]

[a] *Australian Nuclear Science and Technology Organisation, Lucas Heights, New South Wales, Australia*
[b] *Westinghouse Electric Sweden, Bränslegatan 1, 721 36 Västerås, Sweden*
[c] *Nuclear Futures Institute, Bangor University, Bangor, LL57 1UT, U.K.*
[d] *Materials Science and Technology Division, Los Alamos National Laboratory, PO Box 1663, Los Alamos, NM 87545, U.S.A.*
[e] *Department of Materials, Imperial College London, South Kensington, London, U.K.*

Abstract

By combining experimental observations on Gd doped fuel with a theoretical understanding, the variation in thermal conductivity with Gd concentration and accommodation mechanism has been modelled. Four types of Gd accommodation mechanisms have been studied. In UO_{2-x}, isolated substitutional Gd^{3+} ions are compensated by oxygen vacancies and $\{2Gd_U^{'} : V_O^{\cdot\cdot}\}^{\times}$ defect clusters. In UO_2, isolated substitutional Gd^{3+} ions are compensated by U^{5+} ions and $\{Gd_U^{'} : U_U^{\cdot}\}^{\times}$ defect clusters. The results indicate that defect clusters can be considered as less effective phonon scatterers and therefore result in less thermal conductivity degradation. The thermal conductivity predicted for UO_2 with $\{Gd_U^{'} : U_U^{\cdot}\}^{\times}$ defect clusters is in good agreement with experimental data for UO_2 with 5 wt% Gd_2O_3. This supports the previous theoretical results that Gd is accommodated through defect clusters $\{Gd_U^{'} : U_U^{\cdot}\}^{\times}$ in UO_2 in the presence of excess oxygen.

Keywords: Gd_2O_3-doped UO_2, Thermal conductivity, Gadolinium accommodation mechanism, Molecular dynamics simulations

*Corresponding author
Email address: mqi@ansto.gov.au (M.J. Qin)

1. Introduction

Neutron poisons are commonly added to nuclear fuels to limit the initial reactivity in specified pellets/rods identified within the reactor core at the beginning of the operational cycle. This limiting of reactivity has a beneficial effect on the overall lifetime of the core by enabling the use of higher enrichment fuel, providing more fissionable material that extends useful residency of the fuel. The effectiveness of burnable poisons purposefully decreases over time as the neutron absorbing elements are transmuted into elements with lower neutron cross sections (i.e. are used up). The burnable poison can take the form of pins or plates in the fuel assembly or as an additive to the fuel pellet itself. Boron [1], erbium [2] and gadolinium [3] have all been chosen as burnable absorbers in the past: boron is used out of the pellet either as a pellet coating (e.g. ZrB_2 [1]) or within the assembly, whilst gadolinium and erbium oxide are used as fuel additives, and create some interesting crystal-chemical and energetic issues with regard to the initial impurity accomodation mechanisms and modifications to the fuel during burn-up.

Gd is added in fuel as a sesquioxide (i.e. Gd_2O_3) [4, 5]. Past work, both experimental and theoretical, has shown that trivalent oxides can be accommodated in large molar volumes within the UO_2 crystal lattice [6]. The accommodation mechanism of the sesquioxides in UO_2 varies significantly with the amount of oxygen available during the solution reaction: in UO_{2-x} in the absence of excess oxygen, Gd^{3+} is accommodated by forming a charge compensating oxygen vacancy for every two substitutional Gd ions, resulting in $(U,Gd)O_{2-x}$ [7]. In UO_{2+x} where excess oxygen is present, substitutional Gd^{3+} ions are charge compensated by U^{5+} cations. The solubility of Gd or Er in the presence of excess oxygen is limited by the amount of excess oxygen, whereas in the absence of excess oxygen, solubility is a function of temperature [7].

The thermal conductivity of UO_2 is a key property to understand, for the safe and efficient operation of nuclear fuel [8, 9, 10]. Each fission event produces heat, which is transported through the fuel into the cooling fluid of the power

reactor. Past theoretical work has predicted that temperature [11, 12], radiation damage induced defects [13] and secondary phases [14] have major impacts on the fuel's thermal conductivity.

Any degradation in the thermal conductivity of the fuel will have a significant impact on fuel performance, increasing the centre line temperature in a fuel pellet at the beginning of life and into operation compared to a standard UO_2 pellet. This will have knock-on effects on fission gas release and fission product behaviour. Additionally, not only will the margin to melting of the fuel be reduced as a consequence of the addition of Gd, thereby raising the centre-line temperature, but also by the lower melting point of UO_2-Gd_2O_3 solid solutions compared to UO_2 [15].

Past experimental work has measured the change in thermal conductivity with Gd content [16, 17, 18, 19, 20, 21, 22, 23]. The thermal conductivity was observed to decrease with increasing Gd content at relatively low temperatures, but was independent of the Gd content at temperatures close to 2000 K [19]. Simulated burn-up has been taken into account in UO_2 and (U,Gd)O_2 using soluble fission product elements (Sr, Zr, Y, La, Ce, Nd) [20]. The thermal conductivity was observed to decrease with an increase in the total amount of soluble elements at low temperature, but was almost independent of soluble fission element content at higher temperature [20]. Amaya et al. investigated the effect of hyper-stoichiometry on the thermal conductivity of 10 wt% Gd_2O_3 doped UO_{2+x}, and observed degradation in thermal conductivity with increasing hyper-stoichiometry [17, 18]. The thermal conductivity of irradiated (U,Gd)O_2 has been studied by Amaya et al. [16] and Minato et al. [23]; the thermal conductivity decreased with irradiation, and partly recovered after the thermal diffusivity measurements at high temperatures. The recovery of the thermal conductivity was due to the recovery of the irradiation-induced point defects during the measurements. These experimental observations were explained in terms of phonon-phonon scattering and phonon-point defect scattering [19], as well as phonon-extended defect scattering [23].

However, the link between the change in thermal conductivity and the spe-

cific defect accommodation mechanism has not been considered. There has been recent work to study the nature of point defects in non-stoichiometric UO_2 [24]. Due to the requirement for large supercells and associated computational costs, it is still impractical to use first-principle calculations to investigate the lattice thermal conductivity of actinide mixtures (or UO_2 with additives) with point defects. In this work, the impact of Gd_2O_3 doping on the thermal conductivity of UO_2 due to accommodation by oxygen vacancies and U^{5+} cations is explored using non-equilibrium molecular dynamics simulations and compared to experimentally obtained data.

2. Methodology

2.1. Interatomic potentials

The UO_2 potential form used here [25] combines the Buckingham interatomic potential with a many body embedded atom (EAM) term, so that the energy of an ion i, $E_i(r_{ij})$, is given by

$$E_i(r_{ij}) = \frac{1}{2}\sum_j \phi_{\alpha\beta}(r_{ij}) - G_\alpha \sqrt{\sum_j \frac{n_\beta}{r_{ij}^8}}, \tag{1}$$

where $\phi_{\alpha\beta}(r_{ij})$ is the pair-wise interaction between two atoms i and j, separated by r_{ij}, and G_α, n_β are parameters associated with the many-body term. The pair-wise interaction has both long-range electrostatic, $\phi_C(r_{ij})$, and short-range contributions. The latter are described using Morse, $\phi_M(r_{ij})$, and Buckingham, $\phi_B(r_{ij})$, potential forms, where α and β are used to label the species of atom i and atom j, respectively:

$$\phi_{\alpha\beta}(r_{ij}) = \phi_C(r_{ij}) + \phi_B(r_{ij}) + \phi_M(r_{ij}) \tag{2}$$

$$\phi_C(r_{ij}) = \frac{q_\alpha q_\beta}{4\pi\epsilon_0 r_{ij}} \tag{3}$$

$$\phi_B(r_{ij}) = A_{\alpha\beta}\exp\left(-\frac{r_{ij}}{\rho_{\alpha\beta}}\right) - \frac{C_{\alpha\beta}}{r_{ij}^6} \tag{4}$$

Table 1: Parameters for the pairwise interactions described by Eq. (1-5) [25, 27, 28].

Interaction	$\Phi_B(r_{ij})$			$\Phi_M(r_{ij})$		
$\alpha-\beta$	$A_{\alpha\beta}$(eV)	$\rho_{\alpha\beta}$(Å)	$C_{\alpha\beta}$(eVÅ^6)	$D_{\alpha\beta}$(eV)	$\gamma_{\alpha\beta}$(Å^{-1})	r_0(Å)
U^{5+}-O^{2-}	1155.631	0.3465	0	1.9317	2.0528	2.0709
U^{5+}-U^{5+}	18600	0.2429	0	-	-	-
U^{5+}-U^{4+}	18600	0.2583	0	-	-	-
U^{4+}-O^{2-}	448.7789	0.3878	0	0.6608	2.0582	2.3805
U^{4+}-U^{4+}	18600	0.2747	0	-	-	-
Gd^{3+}-O^{2-}	37562.031	0.1938	0	-	-	-
O^{2-}-O^{2-}	830.2834	0.3529	3.8844	-	-	-

$$\phi_M(r_{ij}) = D_{\alpha\beta}\left[\exp(-2\gamma_{\alpha\beta}(r_{ij}-r^0_{\alpha\beta})) - 2\exp(-\gamma_{\alpha\beta}(r_{ij}-r^0_{\alpha\beta}))\right] \quad (5)$$

where $A_{\alpha\beta}$, $\rho_{\alpha\beta}$, $C_{\alpha\beta}$, $D_{\alpha\beta}$, $\gamma_{\alpha\beta}$, and $r^0_{\alpha\beta}$ are empirical parameters describing the Buckingham and Morse potentials between atom i and atom j. The total charge of the ions $q_\alpha = Z^{eff}_\alpha|e|$ describes the Coulombic contribution ($Z^{eff}_\alpha = 2.2208$ for U^{4+} ions, $Z^{eff}_\alpha = 2.7760$ for U^{5+} ions, $Z^{eff}_\alpha = 1.6656$ for Gd^{3+} ions, and $Z^{eff}_\alpha = -1.1104$ for oxygen anions). The pairwise potential parameters are summarised in Table 1.

The second term in equation (1) uses the EAM model to introduce a subtle many-body perturbation to the more dominant pairwise interactions [25] with potential parameters reported in Table 2. This potential model has already proven to be excellent for modelling thermal and mechanical properties of UO_2 [25, 13]. Additional developments of a Gd-O potential by Rushton and Chroneos [26] and U^{5+} potential by Liu et al. [27, 28] are incorporated in this work.

2.2. Details of the simulation

Five supercell models (UO_2, U4-random, U4-bound, U5-random and U5-bound), representing different Gd accommodation mechanisms, were used to

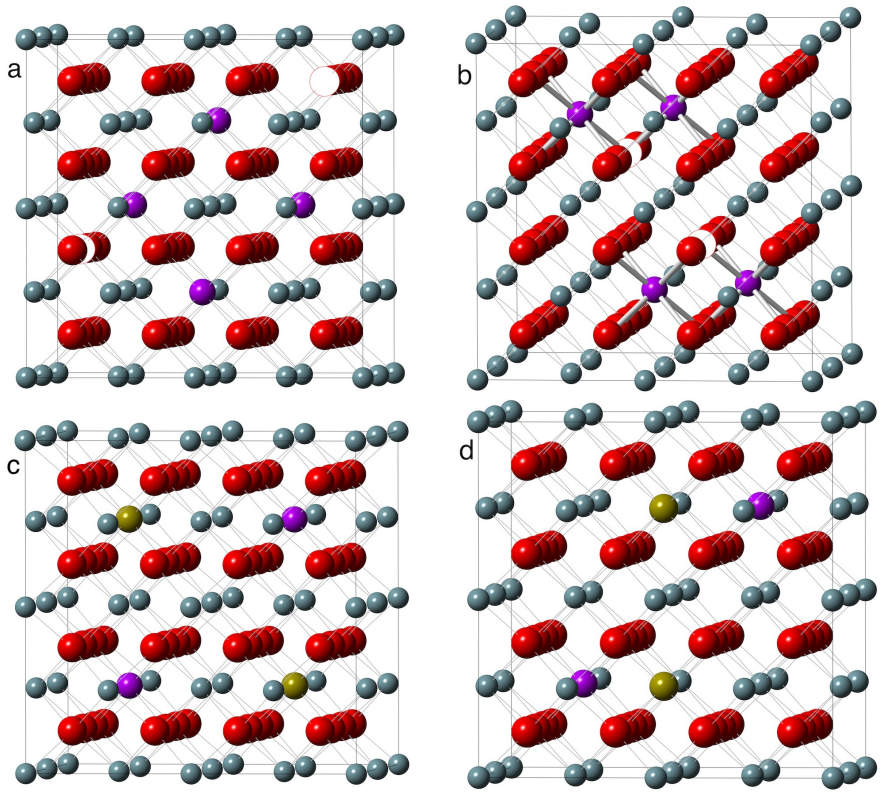

Figure 1: Schematic diagram of a 2×2×2 supercell of UO_2 doped with Gd_2O_3, showing different Gd accommodation mechanisms: (a) isolated Gd^{3+} ions in UO_{2-x} (U4-random), (b) $\{2Gd'_U : V^{\cdot\cdot}_O\}^{\times}$ defect clusters in UO_{2-x} (U4-bound), (c) isolated Gd^{3+} ions in UO_2 (U5-random), (d) $\{Gd'_U : U^{\cdot}_U\}^{\times}$ defect clusters in UO_2 (U5-bound). Oxygen is represented as red, U^{4+} - grey-blue, oxygen vacancy - hollow, Gd - purple, U^{5+} - gold.

investigate the effects on the thermal conductivity of UO_2. U4-random represents isolated Gd^{3+} substitutional defects in UO_{2-x}. It was generated from UO_2 by randomly removing n O^{2-} atoms (leaving behind n oxygen vacancies) and randomly replacing $2n$ U^{4+} atoms with Gd^{3+} atoms (the value of n depends on the doping level). U4-bound represents $\{2Gd_U^{'} : V_O^{\cdot\cdot}\}^{\times}$ defect clusters in UO_{2-x} and was generated from UO_2 by randomly removing n O^{2-} atoms but then replacing the two nearest U^{4+} atoms bounding each removed O^{2-} atom with two Gd^{3+} atoms. Similarly, U5-random also represents isolated Gd^{3+} substitutional atoms in UO_2, and was generated from UO_2 by randomly replacing n U^{4+} atoms with Gd^{3+} atoms and then randomly replacing n U^{4+} atoms with U^{5+} atoms (i.e. charge compensation by U^{5+} not oxygen vacancy). U5-bound represents $\{Gd_U^{'} : U_U^{\cdot}\}^{\times}$ defect clusters in the UO_2 lattice. It was generated from UO_2 by randomly replacing n U^{4+} atoms with U^{5+} atoms and then replacing randomly one of the nearest neighbour U^{4+} atoms of each U^{5+} atom with a Gd^{3+} atom. Figure 1 shows the Gd accommodation mechanisms using (conveniently small) $2\times2\times2$ supercells of UO_2 doped with Gd_2O_3.

The Gd-O potential was originally developed for rare-earth doped CeO_2. To verify its application in the UO_2 system, the lattice parameters of the Gd-doped UO_2 as a function of the Gd content have been calculated as shown in Fig. 2. The lattice parameter of Gd doped UO_2 has been discussed previously with two possible charge compensation mechanisms as the Gd content increases: the creation of the smaller U^{5+} cation and the formation of oxygen vacancies [29, 34, 35]. The smaller U^{5+} cation results in a contraction of the lattice, while the oxygen vacancies were reported to be larger than the O^{2-} ion [34]. The decreasing lattice parameters of U5-bound and U5-random (no oxygen vacancies) with Gd content are consistent with experimental results from Liu et al. [29], Kim et al. [35], Baena et al. [30], and Durazzo et al. [31]. This is due to the smaller U^{5+} cation as compared to the U^{4+} cation. For hypo-stoichiometric (U,Gd)O_2 solid solutions of $(U^{4+}_{1-2x+2y}U^{5+}_{x-2y}Gd^{3+}_x)O_{2-y}$ type, it was shown that the lattice parameter increases with a decrease in the O/M ratio or an increase of oxygen vacancy concentration at constant concentration of Gd [34]. Ohmichi

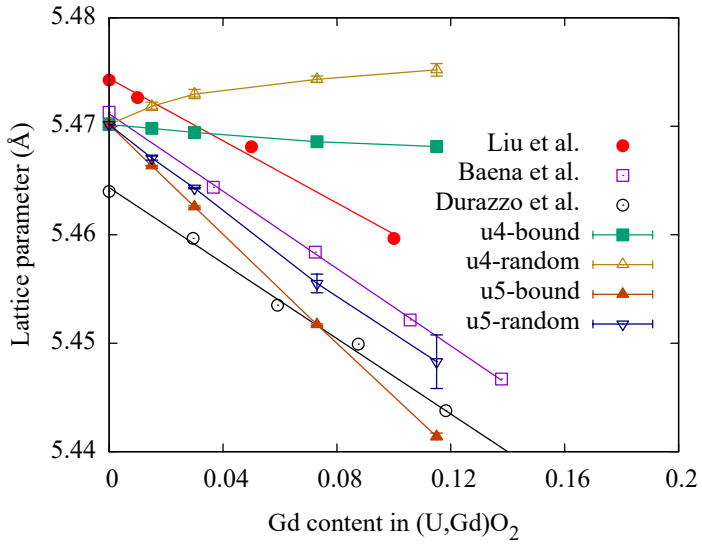

Figure 2: Lattice parameters of $U^{4+}_{1-x}Gd_xO_{2-x/2}$ or $U^{4+}_{1-2x}U^{5+}_xGd_xO_2$ as a function of Gd content in this work, including comparison with the reference results from Liu et al. [29], Baena et al. [30], and Durazzo et al. [31].

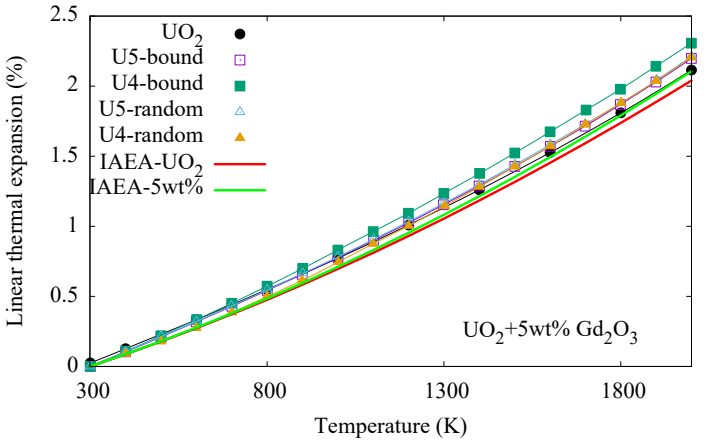

Figure 3: Linear thermal expansion [L(T)-L(300K)]/L(300K) of UO_2+5wt% Gd_2O_3 with the reference results from IAEA [32].

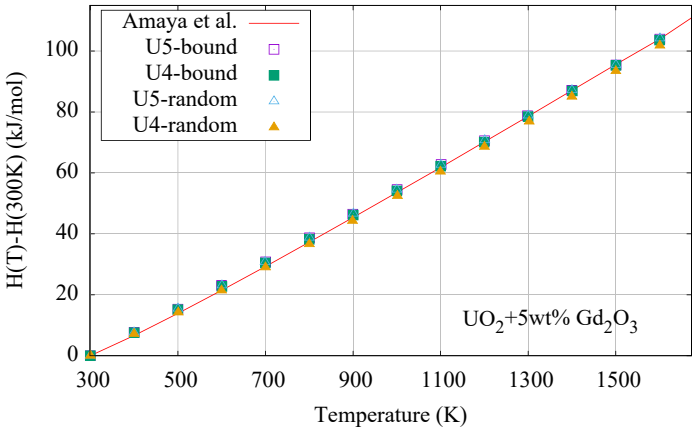

Figure 4: Change in enthalpy of UO_2+5wt% Gd_2O_3 with reference results from Amaya et al. [33].

et al. [34] explained that this increase in the lattice parameter was due to the size of the oxygen vacancy, which is 10% larger than that of the O^{2-} ion. Kim et al. [35] observed a contraction of the lattice for the hypo-stoichiometric sample, but the contraction factor (the slope of the relationship between the lattice parameter and the Gd content) is smaller than those of the hyper-stoichiometric and stoichiometric samples. The authors also explained this observation with the larger size of the oxygen vacancies. The increasing lattice parameter of U4-random (no U^{5+} cations, only oxygen vacancies) agrees with this observation and explanation. The lattice parameter of U4-bound (no U^{5+} cations, only oxygen vacancies), almost constant with Gd content, may indicate smaller oxygen vacancies when bounded with Gd. However, it should be noted that the largest difference in lattice parameters (between U4-random and U5-bound with 8 wt% Gd_2O_3) is only about 0.5%.

Figure 3 shows the linear thermal expansion [L(T)-L(300K)]/L(300K) as a function of temperature calculated for un-doped UO_2 and samples with 5 wt% Gd_2O_3, as well as reference results from IAEA [32]. The linear expansion of the un-doped UO_2 is slightly larger than the IAEA recommended data at the tem-

perature range shown in the figure. As the original potential for un-doped UO_2 was derived based on the Fink model [36] up to higher temperatures, the small difference between the calculated linear expansion and the IAEA data (about 2% at 2000 K) is acceptable. It should be noted that recent experimental investigations on thermal expansion of UO_2 [37] using high-energy XRD indicates a thermal expansion that is systematically slightly higher than the standard reference data of Fink [36]. As such, the doped samples also show slightly larger linear expansion than the IAEA recommended data, being largest for the U4-bound sample (about 10% at 2000 K) and about 5% for the other three samples. Considering the uncertainties associated with the recommended data (about 4% at 2000 K for UO_2 with 5 wt% Gd_2O_3 [32]) and recent experimental data showing higher thermal expansion of UO_2 [37], this difference is acceptable. Figure 4 shows the enthalpy change H(T)-H(300K) as a function of temperature calculated for all samples with 5 wt% Gd_2O_3 and reference results from Amaya et al. [33]. The enthalpy change shows a very small difference and is in excellent agreement with the experimental results.

It can be seen from Figures 2, 3 and 4 that the incorporation of the Gd-O potential originally developed for Gd-doped CeO_2 can predict the experimentally determined thermophysical properties of Gd-doped UO_2, and thus it will be used in this work to simulate the thermal conductivity of Gd_2O_3 doped UO_2.

Thermal conductivities were computed using the non-equilibrium MD (NEMD) approach of Müller-Plathe [38] as implemented in the Large-scale Atomic/Molecular Massively Parallel Simulator (LAMMPS) [39]. A heat flux was imposed along the longest direction of a $5 \times 5 \times 200$ supercell with a 5×5 unit cell cross-section. The mean temperature gradient was measured after the system had reached steady state (normally at $\sim$ 100ps). All simulations were calculated with periodic boundary conditions and a time-step of 1 fs.

Table 2: Parameters for the many-body interactions described by the second term of Eq. (1) [25, 27, 28].

species	G_α(eV Å$^{1.5}$)	n_β(Å^5)
U^{5+}	1.806	3450.995
U^{4+}	1.806	3450.995
O^{2-}	0.690	106.856

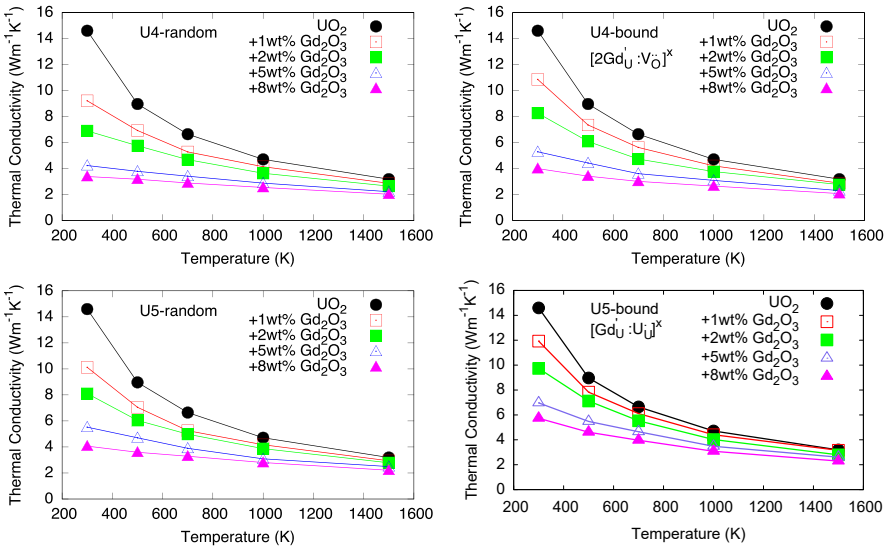

Figure 5: Temperature dependent thermal conductivity of five samples with different Gd_2O_3 contents as indicated in the figure.

3. Results and Discussion

Figure 5 summarizes the calculated thermal conductivities as a function of temperature, K(T), for samples incorporating different accommodation mechanisms and for different Gd_2O_3 concentrations: 0 wt%, 1 wt%, 2 wt%, 5 wt% and 8 wt%. The thermal conductivity functions K(T) are grouped into four groups according to their respective accommodation mechanism, U4-random, U4-bound, U5-random, or U5-bound, which are then shown in separate subfigures. We make the following observations and conclusions: (1) Each thermal conductivity function K(T) decreases with increasing temperature, and would seem to asymptotically approach a (lower) limit, as T increases. As a corollary, as T increases, the rate of decrease of K(T) decreases. (2) The thermal conductivity is a decreasing function of Gd content for all temperatures and all accommodation mechanisms. Consequently, the rate of decrease in K(T) as T increases is smaller for higher Gd contents.

To understand the effects of the Gd accommodation mechanism more clearly, we again show in Figure 6 the thermal conductivities as a function of temperature. However, this time the thermal conductivity curves K(T) are grouped according to the samples' Gd content, so that samples with the same Gd content but different Gd accommodation mechanisms are shown on the same plot. Our main observation is that at low Gd content (1 wt% Gd_2O_3), the difference in the thermal conductivity for the different Gd accommodation mechanisms is relatively small, the largest difference being between U5-bound and U4-random at 300K (about 23%). However, as the Gd content increases, the difference increases (29% and 39% between U5-bound and U4-random at 300K at Gd contents of 2 wt% and 5 wt%, respectively), and becomes quite distinct at a Gd content of 8 wt% (41% between U5-bound and U4-random at 300K).

For all Gd_2O_3 concentrations, the U5-bound sample (i.e. UO_2 containing $\{Gd_U^{'} : U_U\}^{\times}$ defect clusters) shows the highest thermal conductivity, while the U4-random sample (UO_{2-x} containing isolated Gd^{3+}) shows the lowest thermal conductivity, and the thermal conductivities of U5-random (UO_2 containing iso-

lated Gd^{3+}) and U4-bound (UO_{2-x} containing $\{2Gd_U^{'} : V_O^{\cdot\cdot}\}^{\times}$ defect clusters) are in between and very close to each other. It can be seen from Figure 6 that samples with defect clusters (U5-bound and U4-bound) show higher thermal conductivity than those corresponding samples with isolated defects (U5-random and U4-random). The U4-random and U4-bound samples (UO_{2-x}) contain extrinsic charge balancing oxygen vacancies due to the Gd_2O_3 doping. The oxygen vacancies are effective phonon scatterers and will reduce the thermal conductivity [13], however, the thermal conductivity of U4-bound is very close to that of U5-random (no oxygen vacancies). Thus, the defect clusters are less effective phonon scatterers and will reduce thermal conductivity degradation in UO_2.

The experimental thermal conductivity data shown in Figure 6 were measured for a $(U_{0.927}Gd_{0.073})O_2$ sample of 5 wt% Gd_2O_3 concentration [19]. These were thermal conductivity measurements of samples corrected to a theoretical density of 100% K_{th}, by normalising the measured thermal conductivity K_M using the modified Loeb equation [40],

$$K_{th} = \frac{K_M}{1 - P\eta}, \tag{6}$$

where P (0.0443) is the porosity and η an experimental parameter,

$$\eta = 2.6 - 5 \times 10^{-4}(T - 273.15), \tag{7}$$

where T is the temperature in K, as reported by Brandt & Neuer [10].

The oxygen-to-metal ratio (O/M) of the experimental sample was determined to be 2.000 within an experimental error of ± 0.003. Therefore the oxygen vacancy concentration was very low and no more than 0.15 at%, which is negligible compared to the $\sim$ 7.3 at% of U^{5+} ions present in the sample acting as charge compensation for Gd^{3+}. It can be seen from Figure 6, the experimental thermal conductivity (5 wt% Gd_2O_3 concentration) is in excellent agreement with the thermal conductivity of the U5-bound ($\{Gd_U^{'} : U_U^{\cdot}\}^{\times}$ defect clusters in the UO_2) sample. This result is in agreement with previous modelling predictions that the Gd is accommodated by associating itself with a U^{5+} cation

to form stable defect clusters $\{Gd_U^{'} : U_i^{\cdot}\}^{\times}$ in UO_2 with excess oxygen [7].

Thermal conductivity calculated using the FRAPCON-4.0 fuel code [41] is also shown in Figure 6 for comparison (neither burn-up nor irradiation effects were considered for a direct comparison with MD results). At low Gd_2O_3 concentrations (1 wt% and 2 wt%), the thermal conductivity calculated using the FRAPCON-4.0 fuel code is slightly smaller than the MD results. As the Gd_2O_3 concentration is increased to 5 wt%, it becomes larger than the MD results for U4-bound, U4-random and U5-random, but is consistent with the experimental results, and is very close to the MD result for U5-bound. This is even more obvious as the Gd_2O_3 concentration is increased to 8 wt%, for which at temperatures below $\sim$ 700K, the thermal conductivity calculated using the FRAPCON-4.0 fuel code is very close to the MD result for U5-bound, but much larger than the MD results for U4-bound, U4-random and U5-random.

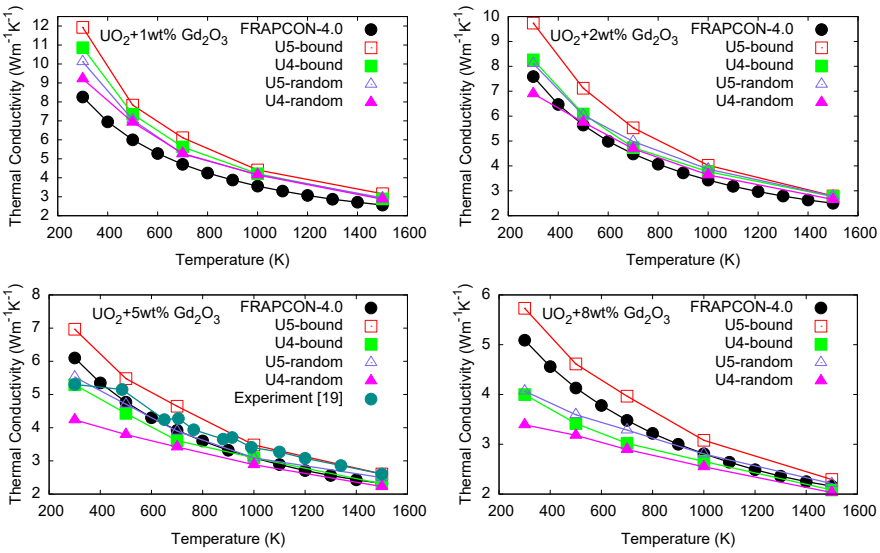

Figure 6: Temperature dependent thermal conductivity of four types of samples, representing different Gd accommodation mechanisms (see text for details), and with different Gd_2O_3 contents. The experimental data were obtained by scaling the measured data to the theoretical value by Hirai and Ishimoto [19].

4. Summary

The effects of Gd accommodation mechanisms and concentration on the thermal conductivity of UO_2 doped with Gd_2O_3 have been investigated using molecular dynamics simulations for four types of Gd accommodation mechanisms: in (U,Gd)O_{2-x}, isolated Gd^{3+} substitutional defects, charge compensated by isolated oxygen vacancies or $\{2Gd_U^{'} : V_O^{\cdot\cdot}\}^{\times}$ defect clusters; and in (U,Gd)O_2, isolated Gd^{3+} substitutional defects, charge compensated by U^{5+} or $\{Gd_U^{'} : U_U^{\cdot}\}^{\times}$ defect clusters. The thermal conductivity was observed to decrease systematically with increase in Gd_2O_3 concentrations and temperature. The samples with $\{Gd_U^{'} : U_U^{\cdot}\}^{\times}$ defect clusters show the highest thermal conductivity, while the samples with isolated Gd^{3+} ions forming (U,Gd)O_{2-x} exhibit the lowest values.

This result indicates that defect clusters are less effective phonon scatterers than their corresponding isolated defects, and would therefore result in less thermal conductivity degradation. The reduction in phonon scattering is likely due to a combination of the reduced number of scattering points (as clusters are expected to act as a single scattering point) coupled with the specific effectiveness of the scattering centre.

The experimental thermal conductivity of a UO_2 sample with 5 wt% Gd_2O_3 content was in good agreement with that of the sample with $\{Gd_U^{'} : U_U^{\cdot}\}^{\times}$ defect clusters (U5-bound), which is consistent with previous theoretical results for the Gd accommodation mechanism of defect clusters $\{Gd_U^{'} : U_U^{\cdot}\}^{\times}$ in UO_2 with excess oxygen.

The thermal conductivity calculated using the FRAPCON-4.0 fuel code was also in good agreement with that of the material with $\{Gd_U^{'} : U_U^{\cdot}\}^{\times}$ defect clusters (U5-bound) at high Gd_2O_3 concentrations.

5. Acknowledgements

This work was supported by the Multi-modal Australian Sciences Imaging and Visualisation Environment (MASSIVE) (www.massive.org.au) and the Sci-

entific Computing team at ANSTO.

References

[1] S. C. Middleburgh, D. C. Parfitt, P. R. Blair, R. W. Grimes, Atomic scale modeling of point defects in zirconium diboride, Journal of the American Ceramic Society 94 (7) (2011) 2225–2229.

[2] V. Barchevtsev, V. Artisyuk, H. Ninokata, Concept of erbium doped uranium oxide fuel cycle in light water reactors, Journal of Nuclear Science and Technology 39 (5) (2002) 506–513.

[3] H. Riella, M. Durazzo, M. Hirata, R. Nogueira, UO_2-Gd_2O_3 solid solution formation from wet and dry processes, Journal of Nuclear Materials 178 (2) (1991) 204 – 211.

[4] M. Hirai, J. Davies, R. Williamson, Diffusivities of fission gas species in UO_2 and (U, Gd)O_2 nuclear fuels during irradiation, Journal of nuclear materials 226 (1-2) (1995) 238–251.

[5] K. W. Song, K. S. Kim, J. H. Yang, K. W. Kang, Y. H. Jung, A mechanism for the sintered density decrease of UO_2-Gd_2O_3 pellets under an oxidizing atmosphere, Journal of nuclear materials 288 (2) (2001) 92–99.

[6] S. C. Middleburgh, D. C. Parfitt, R. W. Grimes, B. Dorado, M. Bertolus, P. R. Blair, L. Hallstadius, K. Backman, Solution of trivalent cations into uranium dioxide, Journal of Nuclear Materials 420 (1) (2012) 258–261.

[7] S. C. Middleburgh, R. W. Grimes, K. H. Desai, P. R. Blair, L. Hallstadius, K. Backman, P. V. Uffelen, Swelling due to fission products and additives dissolved within the uranium dioxide lattice, Journal of Nuclear Materials 427 (1–3) (2012) 359 – 363.

[8] C. Ronchi, M. Sheindlin, M. Musella, G. J. Hyland, Thermal conductivity of uranium dioxide up to 2900 k from simultaneous measurement of the

heat capacity and thermal diffusivity, Journal of Applied Physics 85 (2) (1999) 776–789.

[9] S. R. Phillpot, A. El-Azab, A. Chernatynskiy, J. S. Tulenko, Thermal Conductivity of UO_2 Fuel: Predicting Fuel Performance from Simulation, JOM 63 (8) (2011) 77–83.

[10] R. Brandt, G. Neuer, Thermal conductivity and thermal radiation properties of UO_2, J. Non-Equilib. Thermodyn. 1 (1976) 3–23.

[11] P. Lindan, M. Gillan, A molecular dynamics study of the thermal conductivity of CaF_2 and UO_2, Journal of Physics: Condensed Matter 3 (22) (1991) 3929.

[12] K. Gofryk, S. Du, C. Stanek, J. Lashley, X.-Y. Liu, R. Schulze, J. Smith, D. Safarik, D. Byler, K. McClellan, et al., Anisotropic thermal conductivity in uranium dioxide, Nature communications 5 (2014) 4551.

[13] M. J. Qin, M. W. D. Cooper, E. Y. Kuo, M. J. D. Rushton, R. W. Grimes, G. R. Lumpkin, S. C. Middleburgh, Thermal conductivity and energetic recoils in UO_2 using a many-body potential model, Journal of Physics: Condensed Matter 26 (49) (2014) 495401.

[14] M. L. Fullarton, M. J. Qin, M. Robinson, N. A. Marks, D. J. M. King, E. Y. Kuo, G. R. Lumpkin, S. C. Middleburgh, Structure, properties and formation of $PuCrO_3$ and $PuAlO_3$ of relevance to doped nuclear fuels, Journal of Materials Chemistry A 1 (46) (2013) 14633–14640.

[15] T. Yamada, H. Matsuda, M. Yoshimura, Melting and Measurements of Solidification Point of UO_2-Gd_2O_3 Solid Solutions Under Solar Furnace, JOURNAL-HIGH TEMPERATURE SOCIETY 25 (1999) 71–79.

[16] M. Amaya, M. Hirai, H. Sakurai, K. Ito, M. Sasaki, T. Nomata, K. Kamimura, R. Iwasaki, Thermal conductivities of irradiated UO_2 and (U, Gd)O_2 pellets, Journal of Nuclear Materials 300 (1) (2002) 57–64.

[17] M. Amaya, M. Hirai, T. Kubo, Y. Korei, Thermal conductivity measurements on 10 wt% Gd_2O_3 doped UO_{2+x}, Journal of nuclear materials 231 (1) (1996) 29–33.

[18] M. Amaya, M. Hirai, The effects of oxidation on the thermal conductivity of (U, M)O_2 pellets (M= Gd and/or simulated soluble FPs), Journal of nuclear materials 246 (2-3) (1997) 158–164.

[19] M. Hirai, S. Ishimoto, Thermal diffusivities and thermal conductivities of UO_2-Gd_2O_3, Journal of Nuclear Science and Technology 28 (11) (1991) 995–1000.

[20] S. Ishimoto, M. Hirai, K. Ito, Y. Korei, Effects of soluble fission products on thermal conductivities of nuclear fuel pellets, Journal of Nuclear Science and Technology 31 (8) (1994) 796–802.

[21] K. Iwasaki, T. Matsui, K. Yanai, R. Yuda, Y. Arita, T. Nagasaki, N. Yokoyama, I. Tokura, K. Une, K. K. HARADA, Effect of Gd_2O_3 Dispersion on the Thermal Conductivity of UO_2, Journal of Nuclear Science and Technology 46 (7) (2009) 673–676.

[22] S. Fukushima, T. Ohmichi, A. Maeda, H. Watanabe, The effect of gadolinium content on the thermal conductivity of near-stoichiometric (U, Gd)O_2 solid solutions, Journal of Nuclear Materials 105 (2-3) (1982) 201–210.

[23] K. Minato, T. Shiratori, H. Serizawa, K. Hayashi, K. Une, K. Nogita, M. Hirai, M. Amaya, Thermal conductivities of irradiated UO_2 and (U, Gd)O_2, Journal of nuclear materials 288 (1) (2001) 57–65.

[24] F. Bruneval, M. Freyss, J.-P. Crocombette, Lattice constant in nonstoichiometric uranium dioxide from first principles, Phys. Rev. Materials 2 (2018) 023801.

[25] M. W. D. Cooper, M. J. D. Rushton, R. W. Grimes, A many-body potential approach to modelling the thermomechanical properties of actinide oxides, Journal of Physics: Condensed Matter 26 (10) (2014) 105401.

[26] M. Rushton, A. Chroneos, Impact of uniaxial strain and doping on oxygen diffusion in CeO_2, Scientific reports 4 (1) (2014) 6068.

[27] X.-Y. Liu, M. W. D. Cooper, K. J. McClellan, J. C. Lashley, D. D. Byler, B. D. C. Bell, R. W. Grimes, C. R. Stanek, D. A. Andersson, Molecular Dynamics Simulation of Thermal Transport in UO_2 Containing Uranium, Oxygen, and Fission-product Defects, Phys. Rev. Applied 6 (2016) 044015.

[28] X.-Y. Liu, M. W. D. Cooper, K. J. McClellan, J. C. Lashley, D. D. Byler, B. D. C. Bell, R. W. Grimes, C. R. Stanek, D. A. Andersson, Erratum: Molecular Dynamics Simulation of Thermal Transport in UO_2 Containing Uranium, Oxygen, and Fission-Product Defects [Phys. Rev. Applied 6, 044015 (2016)], Phys. Rev. Applied 7 (2017) 059901.

[29] N. Liu, J. Kim, J. Lee, Y.-S. Youn, J.-G. Kim, J.-Y. Kim, J. J. Noël, D. W. Shoesmith, Influence of gd doping on the structure and electrochemical behavior of uo2, Electrochimica Acta 247 (2017) 496 – 504.

[30] A. Baena, T. Cardinaels, K. Govers, J. Pakarinen, K. Binnemans, M. Verwerft, Lattice contraction and lattice deformation of UO_2 and ThO_2 doped with Gd_2O_3, Journal of Nuclear Materials 467 (2015) 135 – 143.

[31] M. Durazzo, F. Oliveira, E. U. de Carvalho, H. Riella, Phase studies in the UO_2-Gd_2O_3 system, Journal of Nuclear Materials 400 (3) (2010) 183 – 188.

[32] IAEA, Thermophysical properties database of materials for light water reactors and heavy water reactors final report of a coordinated research project 1999-2005, Report 1011-4289 92-0-104706-1 (2006).

[33] M. AMAYA, K. UNE, M. HIRAI, Heat Capacity Measurements of $U_{1-y}Gd_yO_2$ (y=0–0.27) from 325 to 1,673 K, Journal of Nuclear Science and Technology 41 (2) (2004) 108–115.

[34] T. Ohmichi, S. Fukushima, A. Maeda, H. Watanabe, On the relation between lattice parameter and O/M ratio for uranium dioxide-trivalent rare

earth oxide solid solution, Journal of Nuclear Materials 102 (1) (1981) 40 – 46.

[35] J. Kim, J. Lee, Y.-S. Youn, N. Liu, J.-G. Kim, Y.-K. Ha, S.-E. Bae, D. W. Shoesmith, J.-Y. Kim, The combined influence of gadolinium doping and non-stoichiometry on the structural and electrochemical properties of uranium dioxide, Electrochimica Acta 247 (2017) 942 – 948.

[36] J. Fink, Thermophysical properties of uranium dioxide, Journal of Nuclear Materials 279 (1) (2000) 1 – 18.

[37] M. Guthrie, C. Benmore, L. Skinner, O. Alderman, J. Weber, J. Parise, M. Williamson, Thermal expansion in UO_2 determined by high-energy X-ray diffraction, Journal of Nuclear Materials 479 (2016) 19 – 22.

[38] F. Müller-Plathe, A simple nonequilibrium molecular dynamics method for calculating the thermal conductivity, The Journal of Chemical Physics 106 (14) (1997) 6082–6085.

[39] S. Plimpton, Fast parallel algorithms for short-range molecular dynamics, Journal of Computational Physics 117 (1) (1995) 1 – 19.

[40] A. L. Loeb, Thermal conductivity: Viii, a theory of thermal conductivity of porous materials, Journal of the American Ceramic Society 37 (2) (1954) 96–99.

[41] K. J. Geelhood, W. G. Luscher, P. A. Raynaud, I. E. Porter, FRAPCON-4.0: A computer Code for the Calculation of Steady-State, Thermal-Mechanical Behavior of Oxide Fuel Rods for High Burnup, Pacific Northwest National Laboratory, pnnl-19418, vol.1 rev.2 Edition (September 2015).